ISSN 0005-1179 (print), ISSN 1608-3032 (online), Automation and Remote Control, 2023, Vol. 84, No. 3, pp. 317–330.
Trapeznikov Institute of Control Sciences, Russian Academy of Sciences, 2023.

Inverse Kinematics of a 5-Dof Hybrid Manipulator

A. V. Antonov[*,a] **and A. S. Fomin**[*,b]

[*] *Mechanical Engineering Research Institute of the Russian Academy of Sciences (IMASH RAN), Moscow, Russia*
[a] *antonov.av@imash.ru,* [b] *alexey-nvkz@mail.ru*

Received August 22, 2022
Revised October 23, 2022
Accepted October 26, 2022

Abstract—Control of any robotic system cannot be executed without a preliminary solution of the inverse kinematic problem. This problem implies determining the control actions of the actuators required to perform a given motion trajectory and embedded into the control system. The current study considers the inverse kinematics of a hybrid (parallel-serial) manipulator with five degrees-of-freedom (5-DOF). The article first briefly describes the manipulator structure, which includes 3-DOF parallel and 2-DOF serial parts, and then explains an algorithm for solving the inverse kinematics. The algorithm relies on the product-of-exponentials (PoE) formula applied to an equivalent manipulator with a serial structure. The proposed algorithm results in a closed-form solution with no assumptions about the manipulator geometry. A case study confirms the algorithm correctness. The method for solving the inverse kinematic problem can be adapted for other hybrid manipulators.

Keywords: manipulator, parallel-serial (hybrid) structure, kinematic analysis, inverse kinematics, twist, PoE formula

DOI: 10.25728/arcRAS.2023.65.26.001

1. INTRODUCTION

Hybrid manipulators—mechanical devices that consist of several kinematic chains with a parallel and/or serial structure—serve as a basis for many robotic systems [1]. The advanced characteristics of these manipulators include an increased workspace [2] and the ability to pass over or avoid singular configurations [3].

The current article considers a class of hybrid manipulators with five degrees-of-freedom (DOFs), in which a serial kinematic chain is stacked over the parallel one. There are several known manipulators of this type, for example: CaHyMan—a manipulator with a 3-DOF parallel part and a 2-DOF serial part [4]; a machine tool with a 2-DOF parallel part and a 3-DOF serial part [5]; a polishing machine with a 3-DOF parallel module, which provides a vertical motion and a rotation about the horizontal axes, and a 2-DOF serial module for positioning about these axes [6].

Within the control problem of robotic systems (in particular, the hybrid manipulators), one has to find a solution to the inverse kinematic problem (inverse positioning problem). This problem implies determining displacements of the actuators required to perform a given motion trajectory of the output link. The problem is crucial because its solution is embedded directly into the manipulator control system.

Multiple studies have proposed methods for solving the inverse kinematics of hybrid manipulators. One of the first works in this field was [7], where the problem solution involved solving three sextic algebraic equations; the solution was found by numerical methods. The author of [8] matched the initial hybrid manipulator with an equivalent serial one; the closed-form solution was

found from the kinematic relations, derived by the classical Denavit-Hartenberg method [9, p. 506] and homogeneous matrices. A similar Denavit-Hartenberg method was applied to other hybrid manipulators in [10] (together with a geometrical approach) and [5, 11]. Work [12] also represented the initial hybrid manipulator as an equivalent serial one, but its authors used the product-of-exponentials (PoE) formula [9, p. 119] instead of the Denavit-Hartenberg method. Papers [13, 14] implemented this formula too. Structural and geometrical features of the manipulators in the mentioned studies [12–14] allowed their authors to find a closed-form solution to the inverse kinematics. Such features, together with the kinematic decoupling between the translational and rotational motions of the output link, allowed the authors of [15] to consider the serial and parallel parts of the manipulator separately and get a simplified solution. Papers [3, 16–19] analyzed kinematics of other manipulators: most algorithms relied on algebraic or geometric approaches specific to each manipulator.

Earlier, [1] introduced several novel hybrid manipulators, but the inverse kinematics, related directly to the manipulator control problem, was solved for only one of them [20]. The current study continues these articles and considers the inverse kinematics of another hybrid manipulator, described in the subsequent section.

The article has the following organization. Section 2 describes the manipulator structure. Section 3 develops an algorithm for solving the inverse positioning problem, and Section 4 considers a numerical example, which implements the proposed algorithm. Section 5 discusses the algorithm features and briefly compares it with other studies. Section 6 summarizes the results and mentions directions for future research. The article also includes two appendices: Appendix A outlines the theoretical foundations behind the proposed algorithm, and Appendix B contains expressions for coefficients used in equations.

2. MANIPULATOR STRUCTURE

Figure 1 illustrates the kinematic scheme of the considered manipulator and has the following notations: *1*—base; *2*, . . . , *5*—intermediate links; *6*—platform; *7*—carriage; *8*—output link. The manipulator includes a parallel part, formed by links *1*, . . . , *6*, and a serial part, formed by links *7* and *8*. Intermediate links *2*, . . . , *5* are coupled with base *1* and platform *6* by revolute (R) joints; links *2* and *3* are coupled by a revolute joint, and links *4* and *5*—by a prismatic (P) joint. Thus, there are two RRR and two RPR kinematic chains between platform *6* and base *1*. All the revolute joints mentioned above have parallel axes—such a structure provides platform *6* with a 3-DOF

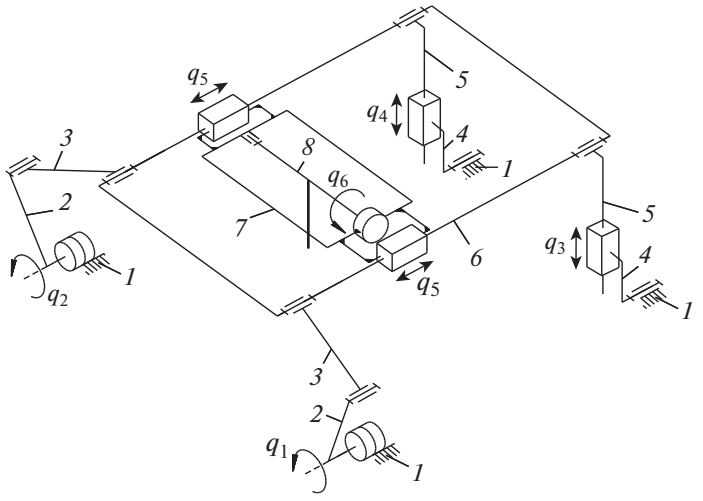

Fig. 1. Kinematic scheme of the considered manipulator.

planar motion. Carriage *7* couples with platform *6* by a prismatic pair and with output link *8* by a revolute one; thus, output link *8* has two DOFs relative to platform *6* and five DOFs relative to base *1*. Output link *8* misses one DOF—rotation about the axis orthogonal to the axes of all the revolute joints. Therefore, we can consider output link *8* has three translational and two rotational DOFs.

In Fig. 1, parameters $q_1, \ldots, q_6$ represent the actuated (controlled) joints of the manipulator:

- q_1 and q_2 correspond to the actuator rotations in chains RRR;
- q_3 and q_4 correspond to the actuator translations in chains RPR;
- q_5 corresponds to the actuator translation of carriage *7*;
- q_6 corresponds to the actuator rotation of output link *8*.

One can see the manipulator is redundantly actuated: four actuators displace platform *6* relative to base *1*, while it has three DOFs. Although such a structure requires coordinated operation of the actuators, this redundancy allows increasing the manipulator stiffness and excluding singular configurations, inherent to parallel manipulators [21]. Furthermore, the fourth kinematic chain makes the manipulator symmetric and increases its workspace dimensions for operations with long-length objects, and these operations are one application of the considered manipulator [1].

3. INVERSE KINEMATICS

The inverse kinematic problem aims to determine displacements in the actuated joints when the output link configuration is given. Hence, we should first consider how to describe these displacements and configuration. We can represent the former by vector $\mathbf{q} = \begin{bmatrix} q_1 & \ldots & q_6 \end{bmatrix}^{\mathrm{T}} \in \mathbb{R}^6$ of actuated coordinates, which correspond to the previous section. Configuration of the output link can be described by vector $\mathbf{p}_S \in \mathbb{R}^3$, which defines a position of some point S on the output link, and unit vector $\hat{\mathbf{n}} \in \mathbb{R}^3$, $\|\hat{\mathbf{n}}\|_2 = 1$, which defines its orientation (Fig. 2a). Parameters $\mathbf{p}_S$ and $\hat{\mathbf{n}}$ are set relative to stationary reference frame $OXYZ$, located on the manipulator base. Since the output link has only two rotational DOFs, vector $\hat{\mathbf{n}}$ suffices to describe its orientation (there is no need to use a rotation matrix).

Thus, the inverse kinematics has reduced to finding vector-function $\mathbf{f}\colon \mathbb{R}^3 \times \mathbb{R}^3 \to \mathbb{R}^6$:

$$\mathbf{q} = \mathbf{f}(\mathbf{p}_S, \hat{\mathbf{n}}), \quad \|\hat{\mathbf{n}}\|_2 = 1. \tag{1}$$

We can represent a method for solving the inverse kinematics as follows.

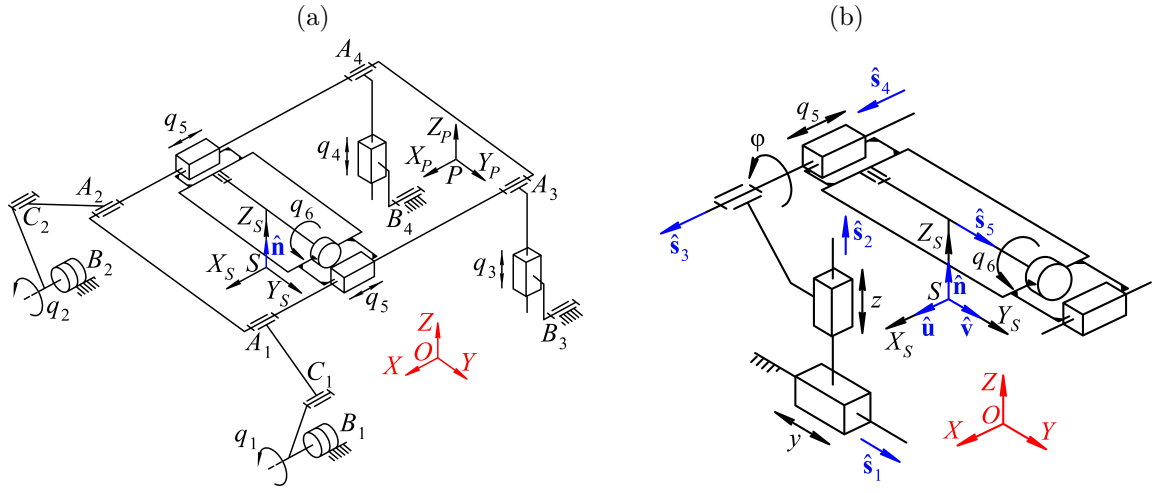

Fig. 2. Kinematic analysis: (a)—reference frames and actuated coordinates; (b)—equivalent kinematic chain with a serial structure.

According to the manipulator structure, the platform performs a planar motion with three DOFs. We can imagine the platform couples to the base by a "virtual" *PPR* kinematic chain; the axes of the prismatic pairs are parallel to the motion plane, and the axis of the revolute pair is orthogonal to it (Fig. 2b). Thus, we can consider a connection between the base and the output link as an equivalent serial kinematic chain with a *PPRPR* structure. As we will see next, such a representation allows using familiar methods, relevant for serial manipulators, to the hybrid manipulator.

Let $SX_SY_SZ_S$ be a reference frame attached to the output link. We can define the frame configuration relative to frame $OXYZ$ by matrix $\mathbf{T}_S \in SE(3)$:

$$\mathbf{T}_S = \begin{bmatrix} \hat{\mathbf{u}} & \hat{\mathbf{v}} & \hat{\mathbf{n}} & \mathbf{p}_S \\ 0 & 0 & 0 & 1 \end{bmatrix}, \tag{2}$$

where $\hat{\mathbf{u}}$ and $\hat{\mathbf{v}}$ are unit vectors, which form a right-hand orthonormal system with vector $\hat{\mathbf{n}}$; as we will see later, directions of these two vectors do not affect the inverse kinematics and can be selected arbitrarily.

Considering the *PPRPR* serial kinematic chain mentioned above, we can use the PoE formula to express matrix $\mathbf{T}_S$ (see Appendix A and equation (A.2)):

$$\mathbf{T}_S = \left(\prod_{i=1}^{5} e^{[\boldsymbol{\xi}_i]\theta_i} \right) \mathbf{M}_S, \tag{3}$$

where $\mathbf{M}_S \in SE(3)$ is a matrix, which defines position and orientation of the output link in some initial configuration of the manipulator; i is an index number of a chain joint, counting from the base, $i = 1, \ldots, 5$; $\boldsymbol{\xi}_i \in \mathbb{R}^6$ is a unit twist, corresponding to the axis of the ith joint in the manipulator initial configuration; $[\boldsymbol{\xi}_i]$ is a matrix representation of twist $\boldsymbol{\xi}_i$ according to equations (A.1) and (A.3); θ_i is a displacement in the ith joint.

For the considered *PPRPR* chain, twists $\boldsymbol{\xi}_i$ and displacements θ_i will have the following expressions according to equation (A.1) and Fig. 2b:

$$\boldsymbol{\xi}_1 = \begin{bmatrix} \mathbf{0}_{3\times1} \\ \hat{\mathbf{s}}_1 \end{bmatrix}, \quad \boldsymbol{\xi}_2 = \begin{bmatrix} \mathbf{0}_{3\times1} \\ \hat{\mathbf{s}}_2 \end{bmatrix}, \quad \boldsymbol{\xi}_3 = \begin{bmatrix} \hat{\mathbf{s}}_3 \\ \mathbf{r}_3 \times \hat{\mathbf{s}}_3 \end{bmatrix}, \quad \boldsymbol{\xi}_4 = \begin{bmatrix} \mathbf{0}_{3\times1} \\ \hat{\mathbf{s}}_4 \end{bmatrix}, \quad \boldsymbol{\xi}_5 = \begin{bmatrix} \hat{\mathbf{s}}_5 \\ \mathbf{r}_5 \times \hat{\mathbf{s}}_5 \end{bmatrix}, \tag{4}$$

$$\theta_1 = y, \quad \theta_2 = z, \quad \theta_3 = \varphi, \quad \theta_4 = q_5, \quad \theta_5 = q_6, \tag{5}$$

where $\hat{\mathbf{s}}_1, \ldots, \hat{\mathbf{s}}_5$ are unit vectors parallel to the axes of the corresponding joints; $\mathbf{r}_3$ and $\mathbf{r}_5$ are vectors, which define coordinates of arbitrary points on the axes of the corresponding joints; y and z are platform translations along vectors $\hat{\mathbf{s}}_1$ and $\hat{\mathbf{s}}_2$ (the choice of such notations will become clear later); φ is a platform rotation along the axis defined by vector $\hat{\mathbf{s}}_3$.

Parameters $\mathbf{M}_S$, $\hat{\mathbf{s}}_1, \ldots, \hat{\mathbf{s}}_5$, $\mathbf{r}_3$, and $\mathbf{r}_5$ depend on the manipulator design and location of frames $OXYZ$ and $SX_SY_SZ_S$, so we can consider them as known. Thus, for given matrix $\mathbf{T}_S$, equation (3) represents a system of equations with variables θ_i, $i = 1, \ldots, 5$, defined in equation (5). To simplify the solution without loss of generality, we can place frame $OXYZ$ such that axis OX is orthogonal to the plane, which is parallel to the axes of both P pairs of the *PPR* "virtual" kinematic chain (Fig. 2b). In this case, we can direct these axes parallel to axes OY and OZ, so we get:

$$\hat{\mathbf{s}}_1 = \begin{bmatrix} 0 & 1 & 0 \end{bmatrix}^{\mathrm{T}}, \quad \hat{\mathbf{s}}_2 = \begin{bmatrix} 0 & 0 & 1 \end{bmatrix}^{\mathrm{T}}, \quad \hat{\mathbf{s}}_3 = \begin{bmatrix} 1 & 0 & 0 \end{bmatrix}^{\mathrm{T}}. \tag{6}$$

Let us substitute equations (2) and (4)–(6) into equation (3) and consider the equation that corresponds to the first row and the third column of equation (3). This equation depends only on variable q_6 and has the following expression:

$$a_1 \cos q_6 + b_1 \sin q_6 + c_1 = 0, \tag{7}$$

where a_1, b_1, and c_1 are coefficients, which are known when solving the inverse kinematics and given in Appendix B.

We can find a solution of equation (7) as follows [22, p. 29]:

$$q_6 = 2\arctan\frac{b_1 \pm \sqrt{a_1^2 + b_1^2 - c_1^2}}{a_1 - c_1}. \tag{8}$$

The equation above has a real solution if the expression under the radical is non-negative. According to Appendix B, this expression depends only on variable n^x, which is a projection of vector $\hat{\mathbf{n}}$ onto axis OX. Therefore, before computing variable q_6, we should first check that this expression is non-negative for all values of n^x or at least the values, which are considered when solving the inverse kinematics. Section 4 will present an example of such an analysis.

The sign in the numerator of equation (8) corresponds to different solutions q_6. The arctan function has two different solutions in a general case, but these two solutions will correspond to the same value of q_6, because the right side of equation (8) is multiplied by two. As a result, we get two different solutions q_6, which depend on the sign ahead of the radical in equation (8).

Next, we will look at equations corresponding to the second and the third rows and the third column of equation (3). We can rewrite these equations in the form similar to equation (7):

$$\begin{aligned} a_2\cos\varphi + b_2\sin\varphi + c_2 = 0,\\ a_3\cos\varphi + b_3\sin\varphi + c_3 = 0, \end{aligned} \tag{9}$$

where $a_2, \ldots, c_3$ are coefficients, dependent on variable q_6 we found above and given in Appendix B.

We can treat equation (9) as a system of linear equations with respect to two variables $\cos\varphi$ and $\sin\varphi$, where $a_2 = b_3$ and $b_2 = -a_3$ according to Appendix B. With such coefficients, the system has a unique solution in a general case (when $a_2b_3 - a_3b_2 \neq 0$) [22, p. 30]. Next, we can use the atan2 function [9, p. 188] to find angle φ. Each of the two solutions of equation (8) will result in a distinct angle φ.

Now, consider the equation corresponding to the first row and the fourth column of equation (3). This equation is linear with respect to variable q_5:

$$a_4q_5 + b_4 = 0, \tag{10}$$

where a_4 and b_4 are coefficients, dependent on variable q_6 we found above and given in Appendix B.

If $a_4 \neq 0$, equation (10) provides a unique solution for each value of q_6. According to Appendix B, $a_4 = s_4^x$, where s_4^x is a projection of vector $\hat{\mathbf{s}}_4$ onto axis OX, which depends on the manipulator geometry. If this geometry causes a zero projection, vector $\hat{\mathbf{s}}_4$ will be parallel to plane OYZ, as well as vectors $\hat{\mathbf{s}}_1$ and $\hat{\mathbf{s}}_2$. These three vectors correspond to the axes of the prismatic pairs in the equivalent kinematic chain (Fig. 2b), so we get a manipulator structure, where the axes of three prismatic pairs are parallel to the common plane. In such a structure, there is an infinite number of combinations between translations q_5, y, and z, which also corresponds to an infinite number of solutions to equation (10). This case, however, has only a theoretical interest, because we can always design a physical manipulator with $s_4^x \neq 0$.

Finally, we can consider the equations that correspond to the second and the third rows and the fourth column of equation (3). These equations are linear with respect to variables y and z, and they look similar to equation (10):

$$\begin{aligned} a_5y + b_5 = 0,\\ a_6z + b_6 = 0, \end{aligned} \tag{11}$$

where $a_5, \ldots, b_6$ are coefficients, dependent on variables q_6, φ, and q_5 we found above and given in Appendix B.

This Appendix shows that $a_5 = a_6 = 1$, so equation (11) also has a unique solution for each value of variable q_6.

Thus, we have found all unknowns θ_i, $i = 1, \ldots, 5$, and variables q_5 and q_6 for the given configuration of the output link, defined by matrix $\mathbf{T}_S$. To find remaining unknowns $q_1, \ldots, q_4$, we can use the PoE formula again and write equation (A.2) for $i = 1, 2$, and 3. Let $PX_PY_PZ_P$ be a platform reference frame, whose configuration relative to base frame $OXYZ$ is determined by matrix $\mathbf{T}_P$, equal to known matrix $\mathbf{M}_P$ in the initial configuration of the platform. According to equation (A.2), we can write:

$$\mathbf{T}_P = \left(\prod_{i=1}^{3} e^{[\boldsymbol{\xi}_i]\theta_i} \right) \mathbf{M}_P, \tag{12}$$

where $\boldsymbol{\xi}_i$ and θ_i correspond to equations (4) and (5).

Parameters θ_1, θ_2, and θ_3 correspond to parameters y, z, and φ found earlier, so we can use equation (12) to compute matrix $\mathbf{T}_P$. Next, we use the equation below to calculate coordinates $\mathbf{p}_{Aj}$, $j = 1, \ldots, 4$, of points A_j, which correspond to the platform revolute joints (Fig. 2a):

$$\begin{bmatrix} \mathbf{p}_{Aj} \\ 1 \end{bmatrix} = \mathbf{T}_P \begin{bmatrix} \mathbf{r}_{Aj} \\ 1 \end{bmatrix}, \quad j = 1, \ldots, 4, \tag{13}$$

where $\mathbf{r}_{Aj}$ are coordinates of points A_j in platform frame $PX_PY_PZ_P$; these coordinates depend on the manipulator design, and they are considered to be known.

After finding coordinates $\mathbf{p}_{Aj}$, we compute actuated coordinates q_3 and q_4 as distances between points A_j and B_j, $j = 3, 4$, where points B_j correspond to the base revolute joints (Fig. 2a):

$$q_j = \sqrt{(\mathbf{p}_{Aj} - \mathbf{p}_{Bj})^2}, \quad j = 3, 4, \tag{14}$$

where $\mathbf{p}_{Bj}$ are coordinates of points B_j in base frame $OXYZ$; these coordinates depend on the manipulator design, and they are considered to be known (we assume without loss of generality that points A_j and B_j are in a plane, orthogonal to the axes of the revolute joints in the jth chain, for each $j = 1, \ldots, 4$).

To find remaining actuated coordinates q_1 and q_2, we first compute coordinates $\mathbf{p}_{Cj}$ of points C_j, $j = 1, 2$, which correspond to the intermediate revolute joints in the RPR chains (Fig. 2a). Since we assumed that axis OX is parallel to the axes of the R joints, we can write the following expressions:

$$\begin{aligned} \left(p^y_{Aj} - p^y_{Cj}\right)^2 + \left(p^z_{Aj} - p^z_{Cj}\right)^2 &= l^2_{AjCj}, \\ \left(p^y_{Bj} - p^y_{Cj}\right)^2 + \left(p^z_{Bj} - p^z_{Cj}\right)^2 &= l^2_{BjCj}, \end{aligned} \qquad j = 1, 2, \tag{15}$$

where $p^y_{Aj}, \ldots, p^z_{Cj}$ are the corresponding components of vectors $\mathbf{p}_{Aj}$, $\mathbf{p}_{Bj}$, and $\mathbf{p}_{Cj}$; l_{AjCj} and l_{BjCj} are the lengths of links A_jC_j and B_jC_j, respectively.

For each $j = 1, 2$, equation (15) represents a system of two quadratic equations with respect to two variables p^y_{Cj} and p^z_{Cj}. Subtracting one equation from another, we can express p^z_{Cj} in terms of p^y_{Cj}:

$$p^z_{Cj} = a_7 p^y_{Cj} + b_7, \quad j = 1, 2, \tag{16}$$

where a_7 and b_7 are known coefficients given in Appendix B.

Substituting equation (16) into any equation of equation (15), we get a quadratic equation with respect to variable p^y_{Cj}:

$$a_8(p^y_{Cj})^2 + b_8 p^y_{Cj} + c_8 = 0, \quad j = 1, 2, \tag{17}$$

where a_8, b_8, and c_8 are known coefficients given in Appendix B.

The expression above allows us to obtain two solutions for variable p^y_{Cj} in a general case, and next we find p^z_{Cj} using equation (16). Note that quadratic equation (17) has a real solution if and only if it is possible to assemble the kinematic chain of the manipulator, i.e., when $\|\mathbf{p}_{Aj} - \mathbf{p}_{Bj}\|_2 \leqslant l_{AjCj} + l_{BjCj}$. Finally, assuming without loss of generality that actuated coordinate q_j, $j = 1, 2$, is measured from the positive direction of axis Oy, we compute this coordinate as follows:

$$q_j = \operatorname{atan2}\left(p^z_{Cj} - p^z_{Bj}, p^y_{Cj} - p^y_{Bj}\right), \quad j = 1, 2. \tag{18}$$

Equations (8), (10), (14), and (18) allow computing actuated coordinates $\mathbf{q}$ for given coordinates $\mathbf{p}_S$ and $\hat{\mathbf{n}}$ of the output link. Thus, these equations represent the desired vector-function from equation (1), which defines the solution to the inverse kinematic problem for the considered manipulator. The performed analysis shows that this problem can have several distinct solutions (up to eight different combinations of actuated coordinates in a general case), and a solution choice depends on the manipulator design and performed operation. For example, various solutions of equation (17) correspond to different assemblies of the RRR kinematic chains (Fig. 1). If the intermediate revolute joint stays outside the platform limits, the manipulator workspace increases, which can be important for the operations with long-length objects; the dimensions of the manipulator, however, increase too. Furthermore, the choice of the chain assembly affects the singularity loci [23], where the manipulator can lose its stiffness and become uncontrollable. Finally, some assemblies can be infeasible a priori because of the joint limits.

4. NUMERICAL EXAMPLE

Let us consider an example of the inverse kinematic analysis for the manipulator with the following parameters (linear parameters are in mm):

$$\hat{\mathbf{s}}_4 = \begin{bmatrix}1 & 0 & 0\end{bmatrix}^{\mathrm{T}}, \quad \hat{\mathbf{s}}_5 = \begin{bmatrix}0 & 1 & 0\end{bmatrix}^{\mathrm{T}}, \qquad \mathbf{r}_3 = \mathbf{r}_5 = \begin{bmatrix}0 & 0 & 250\end{bmatrix}^{\mathrm{T}},$$

$$\mathbf{r}_{A1} = \mathbf{p}_{B1} = \begin{bmatrix}300 & 150 & 0\end{bmatrix}^{\mathrm{T}}, \qquad \mathbf{r}_{A2} = \mathbf{p}_{B2} = \begin{bmatrix}300 & -150 & 0\end{bmatrix}^{\mathrm{T}},$$

$$\mathbf{r}_{A3} = \mathbf{p}_{B3} = \begin{bmatrix}-300 & 150 & 0\end{bmatrix}^{\mathrm{T}}, \qquad \mathbf{r}_{A4} = \mathbf{p}_{B4} = \begin{bmatrix}-300 & -150 & 0\end{bmatrix}^{\mathrm{T}},$$

$$\mathbf{M}_S = \begin{bmatrix}1 & 0 & 0 & 0\\ 0 & 1 & 0 & 0\\ 0 & 0 & 1 & 150\\ 0 & 0 & 0 & 1\end{bmatrix}, \qquad \mathbf{M}_P = \begin{bmatrix}1 & 0 & 0 & 0\\ 0 & 1 & 0 & 0\\ 0 & 0 & 1 & 250\\ 0 & 0 & 0 & 1\end{bmatrix},$$

$$l_{AjCj} = l_{BjCj} = 100, \quad j = 1, 2.$$

With the geometrical parameters above, the platform and the base are the same size: rectangles $A_1A_2A_4A_3$ and $B_1B_2B_4B_3$ are equal and have a length of 600 mm and a width of 300 mm. In the initial configuration, defined by matrices $\mathbf{M}_S$ and $\mathbf{M}_P$, platform plane $A_1A_2A_4A_3$ is parallel to base

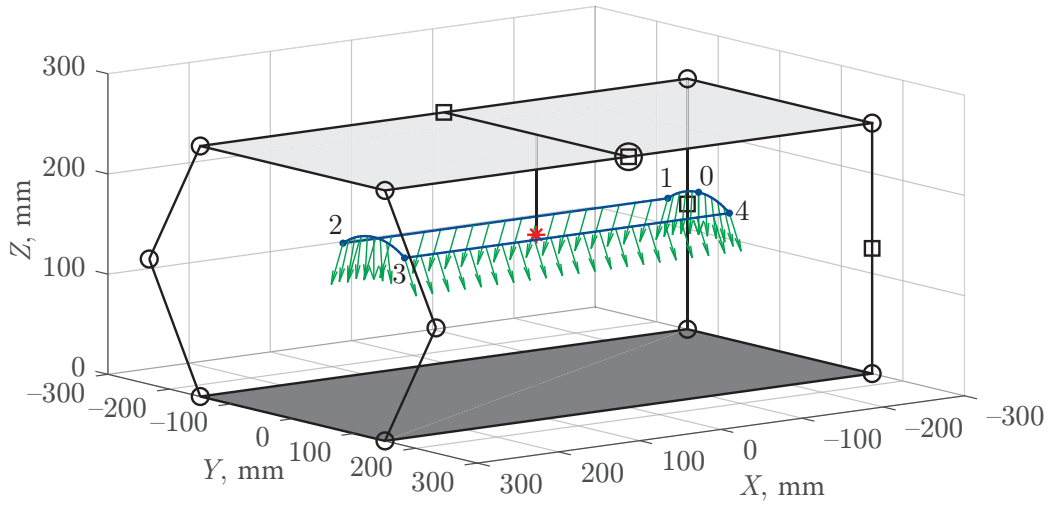

Fig. 3. Manipulator in its initial configuration and the given motion trajectory.

plane OXY and at a height of 250 mm above it. At the same time, point S of the output link is at a height of 150 mm above the base plane (we consider the output link as a 100 mm rod). Figure 3 provides a schematic representation of the manipulator in this configuration.

According to Appendix B and the geometrical parameters above, we get $\sqrt{a_1^2 + b_1^2 - c_1^2} = \sqrt{1 - (n^x)^2}$ in equation (8). Since $|n^x| \leqslant 1$, the expression under the radical is always non-negative, and equation (8) always has a solution. In addition, we have $a_2 b_3 - a_3 b_2 = (\cos q_6)^2$ in equation (9). This expression equals zero when $q_6 = \pm\pi/2$: vector $\hat{\mathbf{n}}$ becomes parallel to axis OX in this case. With such orientation of the output link, it is apparent that the platform can be inclined to the base plane by any angle φ, and the inverse kinematics has an infinite number of solutions. In this regard, one should avoid configurations with $q_6 = \pm\pi/2$ during the trajectory planning.

As an example of the motion trajectory, we will consider a piece-wise curve (Fig. 3), which can relate to processing or monitoring the shape of some long-length object. The trajectory is symmetrical relative to planes OXZ and OYZ. It includes two straight segments (1–2 and 3–4) of 400 mm, which are at a height of 156.6 mm above plane OXY and spaced 100 mm apart, and two arc segments (2–3 and 4–1), whose centers are at a height of 170 mm above plane OXY. Along the entire trajectory, the output link remains parallel to plane OYZ. It keeps the orientation on segments 1–2 and 3–4 and has an angle of $\pm 20^\circ$ with axis OZ; this angle changes between its limit values on segments 2–3 and 4–1 (the arrows in Fig. 3 indicate the tool orientation and correspond to vector $-\hat{\mathbf{n}}$). The motion starts at point 0 in the middle of segment 4–1. The time intervals for segments 0–1, 1–2, 2–3, 3–4, and 4–0 are 1, 4, 2, 4, and 1 s, respectively.

Figure 4 shows plots $\mathbf{q}(t)$, where t is time, which correspond to the solution of the inverse kinematic problem for the geometrical parameters and trajectory set above. The results have a piece-wise form too:

1) For $t \leqslant 1$ s (motion along segment 0–1), the platform goes down and displaces in the negative direction of axis OY, which is indicated by the increase of coordinate q_1 and q_2 and decrease of coordinates q_3 and q_4. The tilt angle of the output link decreases from 0 to -20°, which corresponds to the decrease of coordinate q_6. Coordinate q_5 varies slightly to compensate for the output link inclination and keep point S along axis OX.

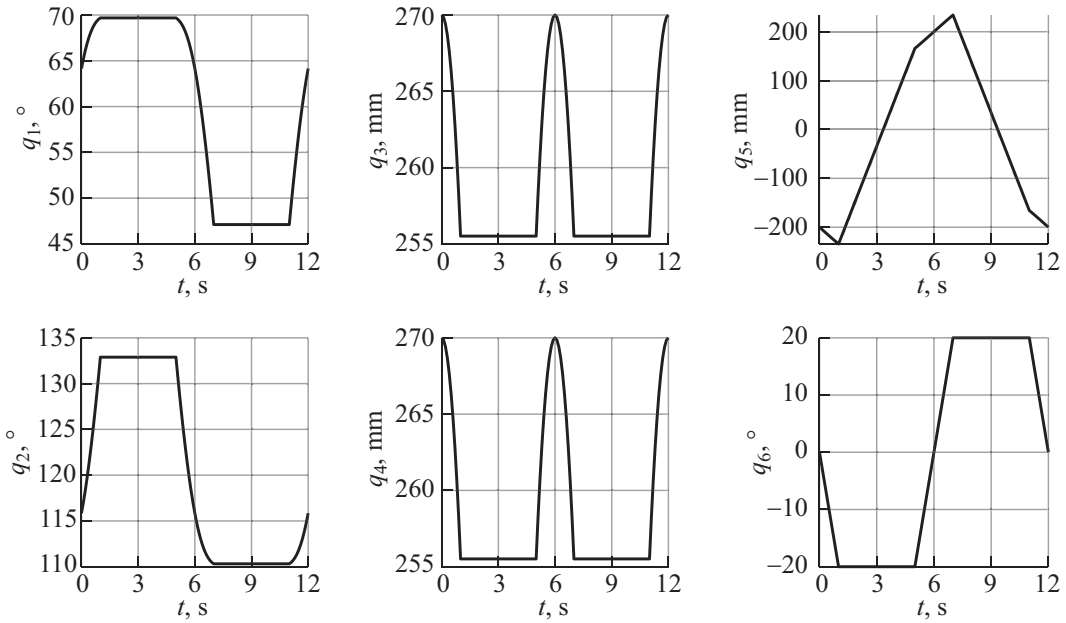

Fig. 4. Solution to the inverse kinematics.

2) For $1 < t \leqslant 5$ s (motion along segment 1–2), the platform is stationary, while the output link keeps its orientation and translates using the actuator of the platform carriage. The values of $q_1, \ldots, q_4$ and q_6 remain constant, and coordinate q_5 changes accordingly.
3) For $5 < t \leqslant 7$ s (motion along segment 2–3), the platform moves in the positive direction of axis OY, which is indicated by the decrease of coordinates q_1 and q_2. In addition, the platform first goes up and then goes down, and we can observe similar behavior in the coordinates q_3 and q_4. The tilt angle of the output link rises from $-20°$ to $+20°$, which corresponds to the changes in coordinate q_6. Coordinate q_5 varies slightly to compensate for the output link inclination and keep point S along axis OX.
4) For $7 < t \leqslant 11$ s (motion along segment 4–5), the actuated coordinates vary similarly to segment 1–2: coordinate q_5 decreases, and other coordinates remain unchanged.
5) For $11 < t \leqslant 12$ s (motion along segment 5–0), the platform goes up and displaces in the negative direction of axis OY, which is indicated by the increase of coordinates $q_1, \ldots, q_4$. The tilt angle of the output link decreases from $+20°$ to 0, which corresponds to the change of coordinate q_6. Coordinate q_5 varies to compensate for the output link inclination and keep point S along axis OX. At the end of the motion, the manipulator returns to the starting point, which is also verified by Fig. 4: $\mathbf{q}(0) = \mathbf{q}(12)$.

The computed values and behavior of the actuated coordinates match the manipulator geometry and the motion trajectory, which confirms the correctness of the proposed inverse kinematic algorithm.

5. DISCUSSION OF RESULTS

The proposed algorithm for solving the inverse kinematics is based on the PoE formulas from equations (3) and (12), which allowed us to find the relations between the given coordinates of the output link and the desired actuated coordinates. This approach requires only a set of parameters ($\boldsymbol{\xi}_i$, $i = 1, \ldots, 5$, $\mathbf{M}_S$, and $\mathbf{M}_P$), which correspond to some arbitrarily selected initial configuration of the manipulator and depend only on the manipulator geometry and location of

the reference frames. We can also consider any geometrical inaccuracies in the axes positions. For example, if the axes of the joints corresponding to actuated coordinates q_5 and q_6 have any offsets, it suffices to adjust the expressions of twists $\boldsymbol{\xi}_4$ and $\boldsymbol{\xi}_5$—the algorithm will work correctly. In addition, Appendix B shows the coefficients are independent of vectors $\hat{\mathbf{u}}$ and $\hat{\mathbf{v}}$ and their expressions in the initial configuration (which corresponds to matrix $\mathbf{M}_S$). Thus, as mentioned earlier, we can select any directions of these vectors.

If we compare the proposed method with other researches, we find there are few studies that applied the PoE formula for solving the inverse kinematic problem of hybrid manipulators. For example, the authors of [13] used this formula only for a serial part of their manipulator; they also made several assumptions about the manipulator geometry, which simplified the solution. In [14], the structural and geometrical features of the manipulator led to simple expressions too, and the solution of the inverse kinematics was found by inverse transformations (inverse matrices $e^{-[\boldsymbol{\xi}_i]\theta_i}$). We should also note paper [12], whose authors applied a similar method and represented the hybrid manipulator as an equivalent serial one, as we did in the current article. The solution of the inverse kinematics was found by solving Paden–Kahan subproblems [24, p. 99], but the authors mentioned that the considered approach was suitable only for specific structures of manipulators. Most of the other studies, including the ones from the introduction, either derived kinematic relations by introducing auxiliary reference frames (using the Denavit–Hartenberg method) or relied on structural features of the considered manipulator and assumptions about its geometry. The algorithm we proposed here does not require any auxiliary reference frames or geometrical assumptions, which makes its application promising for other hybrid manipulators.

6. CONCLUSION

The article has developed an algorithm for solving the inverse kinematic problem of a 5-DOF hybrid manipulator, which consists of the 3-DOF parallel part and the 2-DOF serial part and has a redundant actuation. The proposed algorithm, based on the PoE formula, allows getting the closed-form solution with no assumptions about the manipulator geometry. First, the algorithm computes the coordinates, which define the orientation of the output link. Next, a remaining coordinate of the serial part and the coordinates, which define the position of the output link, are determined. Finally, the algorithm calculates unknown coordinates in the kinematic chains of the parallel part. The considered example has verified the algorithm performance.

The obtained kinematic relations can be used for the forward kinematics, which determines a configuration of the output link for the given actuated coordinates. This problem is of practical importance, because it allows estimating the output link position from the data of the sensors, placed in the manipulator actuators. The considered equations also form a basis for subsequent velocity, singularity, and workspace analyses—these topics represent the future development of the current work. In addition, the proposed techniques can be adapted for other hybrid manipulators.

SUPPLEMENTARY MATERIALS

MATLAB files that correspond to the proposed algorithms are available free online at http://dx.doi.org/10.17632/tp8nx5jhyv.1.

FUNDING

This research was supported by Russian Science Foundation (RSF) under grant no. 22-79-10304, https://rscf.ru/project/22-79-10304/.

APPENDIX A

This Appendix outlines the application of the PoE formula [9] for the kinematic analysis of robotic manipulators.

Let the output link of a manipulator be attached to its base by an open kinematic chain, which consists of n 1-DOF joints (we can represent any multi-DOF joint as a combination of 1-DOF ones). We can associate (unit) twist $\boldsymbol{\xi}_i \in \mathbb{R}^6$ with the ith joint, $i = 1, \ldots, n$:

$$\boldsymbol{\xi}_i = \begin{bmatrix} \boldsymbol{\omega}_i \\ \boldsymbol{\upsilon}_i \end{bmatrix} = \begin{cases} \begin{bmatrix} \hat{\mathbf{s}}_i \\ \mathbf{r}_i \times \hat{\mathbf{s}}_i + h_i \hat{\mathbf{s}}_i \end{bmatrix}, & \text{if } h_i \neq \infty, \\ \begin{bmatrix} \mathbf{0}_{3\times 1} \\ \hat{\mathbf{s}}_i \end{bmatrix}, & \text{if } h_i = \infty, \end{cases} \tag{A.1}$$

where $\boldsymbol{\omega}_i \in \mathbb{R}^3$ is a vector part of the twist; $\boldsymbol{\upsilon}_i \in \mathbb{R}^3$ is a moment part of the twist; $\hat{\mathbf{s}}_i$ is a unit vector parallel to the twist axis; $\mathbf{r}_i$ is a vector that defines coordinates of an arbitrary point on the twist axis; h_i is a pitch of the twist.

Let $SX_SY_SZ_S$ be a reference frame attached to the output link, and let matrix $\mathbf{T}_S \in SE(3)$ define its configuration relative to base reference frame $OXYZ$. Finally, let matrix $\mathbf{M}_S$ describe some initial configuration of the manipulator. In this configuration, we can associate twists $\boldsymbol{\xi}_i$, $i = 1, \ldots, n$, with the chain joints according to equation (A.1). Then, the following relation exists between matrices $\mathbf{T}_S$ and $\mathbf{M}_S$ [9, p. 120]:

$$\mathbf{T}_S = \left(\prod_{i=1}^{n} e^{[\boldsymbol{\xi}_i]\theta_i} \right) \mathbf{M}_S, \tag{A.2}$$

where θ_i is a displacement in the ith joint; $[\boldsymbol{\xi}_i]$ is a matrix representation of twist $\boldsymbol{\xi}_i$:

$$\begin{gathered} [\boldsymbol{\xi}_i] = \begin{bmatrix} \Lambda(\boldsymbol{\omega}_i) & \boldsymbol{\upsilon}_i \\ \mathbf{0}_{1\times 3} & 0 \end{bmatrix} \in se(3), \\ \Lambda(\boldsymbol{\omega}_i) = \Lambda\left(\begin{bmatrix} \omega_i^x \\ \omega_i^y \\ \omega_i^z \end{bmatrix} \right) = \begin{bmatrix} 0 & -\omega_i^z & \omega_i^y \\ \omega_i^z & 0 & -\omega_i^x \\ -\omega_i^y & \omega_i^x & 0 \end{bmatrix} \in so(3). \end{gathered} \tag{A.3}$$

Equation (A.2) represents the product of exponentials $e^{[\boldsymbol{\xi}_i]\theta_i}$:

$$e^{[\boldsymbol{\xi}_i]\theta_i} = \begin{bmatrix} e^{\Lambda(\boldsymbol{\omega}_i)\theta_i} & \left(\mathbf{I}_{3\times 3}\theta_i + (1 - \cos\theta_i)\Lambda(\boldsymbol{\omega}_i) + (\theta_i - \sin\theta_i)\Lambda(\boldsymbol{\omega}_i)^2\right)\boldsymbol{\upsilon}_i \\ \mathbf{0}_{1\times 3} & 1 \end{bmatrix},$$

where $e^{\Lambda(\boldsymbol{\omega}_i)\theta_i}$ corresponds to the rotation matrix about the axis defined by vector $\boldsymbol{\omega}_i$ by angle θ_i:

$$e^{\Lambda(\boldsymbol{\omega}_i)\theta_i} = \mathbf{I}_{3\times 3} + \sin\theta_i \Lambda(\boldsymbol{\omega}_i) + (1 - \cos\theta_i)\Lambda(\boldsymbol{\omega}_i)^2.$$

Initial configuration $\mathbf{M}_S$ and corresponding twists $\boldsymbol{\xi}_i$, $i = 1, \ldots, n$, depend on the manipulator design and location of reference frames $SX_SY_SZ_S$ and $OXYZ$, so these parameters are considered known for the kinematic analysis. Thus, equation (A.2) represents the relationship between joint displacements θ_i and the output link configuration defined by matrix $\mathbf{T}_S$. We can use this equation not only for the forward kinematics (where it is applied generally [9]), but also for the inverse kinematics, which is demonstrated in the present article for the hybrid manipulator.

APPENDIX B

This Appendix contains coefficients of the equations, which are used for solving the inverse kinematic problem:

$$
\begin{aligned}
a_1 &= n_0^x((s_5^y)^2 + (s_5^z)^2) - n_0^y s_5^x s_5^y - n_0^z s_5^x s_5^z,\\
b_1 &= -n_0^y s_5^z + n_0^z s_5^y,\\
c_1 &= n_0^x (s_5^x)^2 + n_0^y s_5^x s_5^y + n_0^z s_5^x s_5^z - n^x,\\
a_2 &= n_0^x(s_5^x s_5^y(1-\cos q_6) + s_5^z \sin q_6) + n_0^y((s_5^y)^2(1-\cos q_6) + \cos q_6)\\
&\quad - n_0^z(s_5^x \sin q_6 - s_5^y s_5^z(1-\cos q_6)),\\
b_2 &= n_0^x(s_5^x s_5^z(\cos q_6 - 1) + s_5^y \sin q_6) - n_0^y(s_5^x \sin q_6 + s_5^y s_5^z(1-\cos q_6))\\
&\quad + n_0^z((s_5^z)^2(\cos q_6 - 1) - \cos q_6),\\
c_2 &= -n^y,\\
a_3 &= n_0^x(s_5^x s_5^z(1-\cos q_6) - s_5^y \sin q_6) + n_0^y(s_5^x \sin q_6 + s_5^y s_5^z(1-\cos q_6))\\
&\quad + n_0^z((s_5^z)^2(1-\cos q_6) + \cos q_6),\\
b_3 &= n_0^x(s_5^x s_5^y(1-\cos q_6) + s_5^z \sin q_6) + n_0^y((s_5^y)^2(1-\cos q_6) + \cos q_6)\\
&\quad - n_0^z(s_5^x \sin q_6 - s_5^y s_5^z(1-\cos q_6)),\\
c_3 &= -n^z,\\
a_4 &= s_4^x,\\
b_4 &= p_{S0}^x(((s_5^y)^2 + (s_5^z)^2)(\cos q_6 - 1) + 1) + p_{S0}^y(s_5^x s_5^y(1-\cos q_6) - s_5^z \sin q_6)\\
&\quad + p_{S0}^z(s_5^x s_5^z(1-\cos q_6) + s_5^y \sin q_6) + r_5^x((s_5^y)^2 + (s_5^z)^2)(1-\cos q_6)\\
&\quad + r_5^y(s_5^x s_5^y(\cos q_6 - 1) + s_5^z \sin q_6) + r_5^z(s_5^x s_5^z(\cos q_6 - 1) - s_5^y \sin q_6) - p_S^x,\\
a_5 &= 1,\\
b_5 &= p_{S0}^x(s_5^x s_5^y(1-\cos q_6)\cos\varphi + s_5^x s_5^z(\cos q_6 - 1)\sin\varphi + s_5^y \sin q_6 \sin\varphi + s_5^z \sin q_6 \cos\varphi)\\
&\quad + p_{S0}^y(-s_5^x \sin q_6 \sin\varphi + (s_5^y)^2(1-\cos q_6)\cos\varphi + s_5^y s_5^z(\cos q_6 - 1)\sin\varphi + \cos q_6 \cos\varphi)\\
&\quad + p_{S0}^z(-s_5^x \sin q_6 \cos\varphi + s_5^y s_5^z(1-\cos q_6)\cos\varphi + (s_5^z)^2(\cos q_6 - 1)\sin\varphi + \cos q_6 \sin\varphi)\\
&\quad + q_5(s_4^y \cos\varphi - s_4^z \sin\varphi) + r_3^y(1-\cos\varphi) + r_3^z \sin\varphi\\
&\quad + r_5^x(s_5^x(\cos q_6 - 1)(s_5^y \cos\varphi - s_5^z \sin\varphi) - s_5^y \sin q_6 \sin\varphi - s_5^z \sin q_6 \cos\varphi\\
&\quad + r_5^y(s_5^x \sin q_6 \sin\varphi + ((s_5^y)^2 \cos\varphi - s_5^y s_5^z \sin\varphi - \cos\varphi)(\cos q_6 - 1))\\
&\quad + r_5^z(s_5^x \sin q_6 \cos\varphi + (s_5^y s_5^z \cos\varphi - (s_5^z)^2 \sin\varphi + \sin\varphi)(\cos q_6 - 1)) - p_S^y,\\
a_6 &= 1,\\
b_6 &= p_{S0}^x(s_5^x s_5^y(1-\cos q_6)\sin\varphi + s_5^x s_5^z(1-\cos q_6)\cos\varphi - s_5^y \sin q_6 \cos\varphi + s_5^z \sin q_6 \sin\varphi)\\
&\quad + p_{S0}^y(s_5^x \sin q_6 \cos\varphi + (s_5^y)^2(1-\cos q_6)\sin\varphi + s_5^y s_5^z(1-\cos q_6)\cos\varphi + \cos q_6 \sin\varphi)\\
&\quad + p_{S0}^z(-s_5^x \sin q_6 \sin\varphi + s_5^y s_5^z(1-\cos q_6)\sin\varphi + (s_5^z)^2(1-\cos q_6)\cos\varphi + \cos q_6 \cos\varphi)\\
&\quad + q_5(s_4^y \sin\varphi + s_4^z \cos\varphi) - r_3^y \sin\varphi + r_3^z(1-\cos\varphi)\\
&\quad + r_5^x(s_5^x(\cos q_6 - 1)(s_5^y \sin\varphi + s_5^z \cos\varphi) + s_5^y \sin q_6 \cos\varphi - s_5^z \sin q_6 \sin\varphi\\
&\quad + r_5^y(-s_5^x \sin q_6 \cos\varphi + ((s_5^y)^2 \sin\varphi + s_5^y s_5^z \cos\varphi - \sin\varphi)(\cos q_6 - 1))\\
&\quad + r_5^z(s_5^x \sin q_6 \sin\varphi + (s_5^y s_5^z \sin\varphi + (s_5^z)^2 \cos\varphi - \cos\varphi)(\cos q_6 - 1)) - p_S^z,
\end{aligned}
$$

$$a_7 = -\frac{p^y_{Aj} - p^y_{Bj}}{p^z_{Aj} - p^z_{Bj}},$$
$$b_7 = \frac{(p^y_{Aj})^2 + (p^z_{Aj})^2 - (p^y_{Bj})^2 - (p^z_{Bj})^2 - l^2_{AjCj} + l^2_{BjCj}}{2(p^z_{Aj} - p^z_{Bj})},$$

$$a_8 = 1 + a_7^2,$$
$$b_8 = -2p^y_{Aj} - 2a_7(p^z_{Aj} - b_7),$$
$$c_8 = (p^z_{Aj} - b_7)^2 - l^2_{AjCj},$$

where p^x_S, p^y_S, p^z_S and n^x, n^y, n^z are the corresponding components of vectors $\mathbf{p}_S$ and $\hat{\mathbf{n}}$; p^x_{S0}, p^y_{S0}, p^z_{S0} and n^x_0, n^y_0, n^z_0 are the same components in the initial configuration of the manipulator (defined by matrix $\mathbf{M}_S$ in equation (3)); $s^x_4, \ldots, s^z_5$ are the corresponding components of vectors $\hat{\mathbf{s}}_4$ and $\hat{\mathbf{s}}_5$.

REFERENCES

1. Ganiev, R.F., Glazunov, V.A., and Filippov, G.S., Urgent Problems of Machine Science and Ways of Solving Them: Wave and Additive Technologies, the Machine Tool Industry, and Robot Surgery, *Journal of Machinery Manufacture and Reliability*, 2018, vol. 47, no. 5, pp. 399–406. https://doi.org/10.3103/S1052618818050059
2. Wen, K., Harton, D., Laliberté, T., and Gosselin, C., Kinematically Redundant (6+3)-dof Hybrid Parallel Robot with Large Orientational Workspace and Remotely Operated Gripper, *Proceedings of the 2019 IEEE International Conference on Robotics and Automation*, IEEE, 2019, pp. 1672–1678. https://doi.org/10.1109/ICRA.2019.8793772
3. Liu, Q. and Huang, T., Inverse Kinematics of a 5-axis Hybrid Robot with Non-singular Tool Path Generation, *Robotics and Computer-Integrated Manufacturing*, 2019, vol. 56, pp. 140–148. https://doi.org/10.1016/j.rcim.2018.06.003
4. Carbone, G. and Ceccarelli, M., A Stiffness Analysis for a Hybrid Parallel-serial Manipulator, *Robotica*, 2004, vol. 22, no. 5, pp. 567–576. https://doi.org/10.1017/S0263574704000323
5. Lai, Y.-L., Liao, C.-C., and Chao, Z.-G., Inverse Kinematics for a Novel Hybrid Parallel–serial Five-axis Machine Tool, *Robotics and Computer-Integrated Manufacturing*, 2018, vol. 50, pp. 63–79. https://doi.org/10.1016/j.rcim.2017.09.002
6. Oba, Y. and Kakinuma, Y., Simultaneous Tool Posture and Polishing Force Control of Unknown Curved Surface Using Serial-parallel Mechanism Polishing Machine, *Precision Engineering*, 2017, vol. 49, pp. 24–32. https://doi.org/10.1016/j.precisioneng.2017.01.006
7. Waldron, K.J., Raghavan, M., and Roth, B., Kinematics of a Hybrid Series-parallel Manipulation System, *Journal of Dynamic Systems, Measurement, and Control*, 1989, vol. 111, no. 2, pp. 211–221. https://doi.org/10.1115/1.3153039
8. Cheng, H.H., Real-time Manipulation of a Hybrid Serial-and-parallel-driven Redundant Industrial Manipulator, *Journal of Dynamic Systems, Measurement, and Control*, 1994, vol. 116, no. 4, pp. 687–701. https://doi.org/10.1115/1.2899268
9. Lynch, K.M. and Park, F.C., *Modern Robotics: Mechanics, Planning, and Control*, Cambridge: Cambridge University Press, 2017. https://doi.org/10.1017/9781316661239
10. Tang, Z. and Payandeh, S., Design and Modeling of a Novel 6 Degree of Freedom Haptic Device, *Proceedings of the 3rd Joint EuroHaptics Conference and Symposium on Haptic Interfaces for Virtual Environment and Teleoperator Systems*, IEEE, 2009, pp. 1941–1946. https://doi.org/10.1109/WHC.2009.4810891
11. Yan, C., Gao, F., and Zhang, Y., Kinematic Modeling of a Serial-parallel Forging Manipulator with Application to Heavy-duty Manipulations, *Mechanics Based Design of Structures and Machines*, 2010, vol. 38, no. 1, pp. 105–129. https://doi.org/10.1080/15397730903455344

12. Sun, P., Li, Y.B., Wang, Z.S., Chen, K., Chen, B., Zeng, X., Zhao, J., and Yue, Y., Inverse Displacement Analysis of a Novel Hybrid Humanoid Robotic Arm, *Mechanism and Machine Theory*, 2020, vol. 147, p. 103743. https://doi.org/10.1016/j.mechmachtheory.2019.103743

13. Yang, G., Chen, W., and Ho, E.H.L., Design and Kinematic Analysis of a Modular Hybrid Parallel-serial Manipulator, *Proceedings of the 7th International Conference on Control, Automation, Robotics and Vision*, IEEE, 2002, vol. 1, pp. 45–50. https://doi.org/10.1109/ICARCV.2002.1234788

14. Tang, C., Zhang, J., and Cheng, S., Kinematics Analysis for a Hybrid Robot in Minimally Invasive Surgery, *Proceedings of the 2009 IEEE International Conference on Robotics and Biomimetics*, IEEE, 2009, pp. 1941–1946. https://doi.org/10.1109/ROBIO.2009.5420534

15. Lee, M.K., Park, K.W., and Choi, B.O., Kinematic and Dynamic Models of Hybrid Robot Manipulator for Propeller Grinding, *Journal of Robotic Systems*, 1999, vol. 16, no. 3, pp. 137–150. https://doi.org/10.1002/(SICI)1097-4563(199903)16:3<137::AID-ROB1>3.0.CO;2-V

16. Pisla, D., Gherman, B., Vaida, C., Suciu, M., and Plitea, N., An Active Hybrid Parallel Robot for Minimally Invasive Surgery, *Robotics and Computer-Integrated Manufacturing*, 2013, vol. 29, no. 4, pp. 203–221. https://doi.org/10.1016/j.rcim.2012.12.004

17. Hu, B., Shi, Y., Xu, L., and Bai, P., Reconsideration of Terminal Constraint/Mobility and Kinematics of 5-DOF Hybrid Manipulators Formed by One 2R1T PM and One RR SM, *Mechanism and Machine Theory*, 2020, vol. 149, p. 103837. https://doi.org/10.1016/j.mechmachtheory.2020.103837

18. Ye, H., Wang, D., Wu, J., Yue, Y., and Zhou, Y., Forward and Inverse Kinematics of a 5-DOF Hybrid Robot for Composite Material Machining, *Robotics and Computer-Integrated Manufacturing*, 2020, vol. 65, p. 101961. https://doi.org/10.1016/j.rcim.2020.101961

19. López-Custodio, P.C., Fu, R., Dai, J.S., and Jin, Y., Compliance Model of Exechon Manipulators with an Offset Wrist, *Mechanism and Machine Theory*, 2022, vol. 167, p. 104558. https://doi.org/10.1016/j.mechmachtheory.2021.104558

20. Antonov, A., Fomin, A., Glazunov, V., Kiselev, S., and Carbone, G., Inverse and Forward Kinematics and Workspace Analysis of a Novel 5-DOF (3T2R) Parallel-serial (Hybrid) Manipulator, *International Journal of Advanced Robotic Systems*, 2021, vol. 18, no. 2, p. 2963. https://doi.org/10.1177/1729881421992963

21. Gosselin, C. and Schreiber, L.-T., Redundancy in Parallel Mechanisms: A Review, *Applied Mechanics Reviews*, 2018, vol. 70, no. 1, p. 010802. https://doi.org/10.1115/1.4038931

22. Waldron, K.J. and Schmiedeler, J., Kinematics, *Springer Handbook of Robotics*, Springer, 2016, pp. 11–36. https://doi.org/10.1007/978-3-319-32552-1_2

23. Liu, S., Qiu, Z., and Zhang, X., Singularity and Path-planning with the Working Mode Conversion of a 3-DOF 3-RRR Planar Parallel Manipulator, *Mechanism and Machine Theory*, 2017, vol. 107, pp. 166–182. https://doi.org/10.1016/j.mechmachtheory.2016.09.004

24. Murray, R.M., Li, Z., and Sastry, S.S., *A Mathematical Introduction to Robotic Manipulation*, Boca Raton: CRC Press, 1994. https://doi.org/10.1201/9781315136370

This paper was recommended for publication by P.V. Pakshin, a member of the Editorial Board